The North African Journal of Scientific Publishing (NAJSP)
مجلة شمال إفريقيا للنشر العلمي (NAJSP)
E-ISSN: 2959-4820
Volume 4, Issue 4, 2026
Page No: 134-146
Website: https://najsp.com/index.php/home/index
SJIFactor 2024: 5.49 معامل التأثير العربي (AIF) 2025: 0.69 ISI 2024: 0.696

Chemoselective Synthesis, DFT Analysis, Molecular Docking, and ADMET Profiling of Ethyl 2-(2-Phenylhydrazinyl) cyclopent-1-ene-1-carboxylate

Abdalhamid Alarafi[1*], Abdullah Gheath[2]
[1]Department of Chemistry, Faculty of Arts and Sciences, University of Benghazi, Al-Abyar, Libya
[2]Department of Chemistry, Faculty of Science, University of Benghazi, Benghazi, Libya

التخليق الكيميائي الانتقائي، وتحليل نظرية الكثافة الوظيفية، والالتحام الجزيئي، وتحديد خصائص ADMET لمركب إيثيل 2-(2-فينيل هيدرازينيل) سيكلوبنت-1-إين-1-كربوكسيلات

عبد الحميد العرفي[1*]، عبدالله غيث[2]
[1]قسم الكيمياء، كلية العلوم والاداب، جامعة بنغازي، الأبيار، ليبيا
[2]قسم الكيمياء، كلية العلوم، جامعة بنغازي، بنغازي، ليبيا

*Corresponding author: abdalhamid.abdallah@uob.edu.ly

Received: July 26, 2026	Accepted: October 05, 2026	Published: October 20, 2026

Copyright: © 2026 by the authors. Submitted for possible open access publication under the terms and conditions of the Creative Commons Attribution (CC BY) license (https://creativecommons.org/licenses/by/4.0/).

Abstract:
The integration of experimental synthesis with computational approaches provides a valuable strategy for investigating the structural, electronic, and biological interaction properties of organic compounds. In the present study, ethyl 2-(2-phenylhydrazinyl) cyclopent-1-ene-1-carboxylate (1) was synthesized through the chemoselective condensation of ethyl 2-oxocyclopentane-1-carboxylate with phenylhydrazine in ethanol. The reaction afforded the target compound as an off-white solid in 19% isolated yield, with preferential reaction at the ketone functionality while preserving the ester group. Density functional theory (DFT) calculations were performed at the B3LYP/6-31G level to investigate molecular geometry, electronic structure, and global reactivity descriptors. The optimized structure exhibited no imaginary vibrational frequencies, with a calculated HOMO–LUMO energy gap of 4.5135 eV and a dipole moment of 2.8675 Debye. Molecular electrostatic potential mapping further identified electron-rich and electron-deficient regions potentially involved in intermolecular interactions. Molecular docking simulations using MOE 2024 were conducted against three bacterial proteins: Escherichia coli DNA gyrase B (6KZV), Staphylococcus aureus penicillin-binding protein 4 (5TW8), and Bacillus subtilis CotA laccase (1OF0). Compound 1 exhibited docking scores of −6.955, −5.839, and −5.081 kcal/mol, respectively, indicating predicted binding interactions within the investigated protein pockets. In silico ADMET assessment revealed favorable physicochemical properties and compliance with established drug-likeness criteria. However, predicted cytochrome P450 inhibition and potential organ-specific toxicity highlighted important pharmacokinetic and safety concerns. Overall, the findings provide a preliminary characterization of the synthesized compound and identify

its potential for further structure-based investigation. Experimental biological evaluation, mechanistic studies, and toxicity assessment are required before any therapeutic relevance can be established.

Keywords: Chemoselective synthesis; Phenylhydrazinyl derivatives; Enamino esters; Density functional theory (DFT); Molecular docking.

الملخص:
يوفر دمج التخليق التجريبي مع الأساليب الحسابية استراتيجية قيّمة لدراسة الخصائص الهيكلية والإلكترونية والتفاعلات البيولوجية للمركبات العضوية. في هذه الدراسة، تم تخليق إيثيل 2-(2-فينيل هيدرازينيل) سيكلوبنت-1-إين-1-كربوكسيلات (1) من خلال التكثيف الكيميائي الانتقائي لإيثيل 2-أوكسوسيكلوبنتان-1-كربوكسيلات مع فينيل هيدرازين في الإيثانول. وقد أسفر التفاعل عن المركب المستهدف كمادة صلبة بيضاء مائلة للصفرة بنسبة 19% من العائد المعزول، مع تفاعل تفضيلي عند وظيفة الكيتون مع الحفاظ على مجموعة الإستر. تم إجراء حسابات نظرية الكثافة الوظيفية (DFT) عند مستوى B3LYP/6-31G لدراسة الهندسة الجزيئية والبنية الإلكترونية ومؤشرات التفاعل العالمية لم يُظهر التركيب المُحسَّن أي ترددات اهتزازية تخيلية، مع فجوة طاقة محسوبة بين أعلى مستوى جزيئي مشغول (HOMO) وأدنى مستوى جزيئي غير مشغول (LUMO) تبلغ 4.5135 إلكترون فولت، وعزم ثنائي قطب يبلغ 2.8675 ديباي. كما حددت خرائط الجهد الكهروستاتيكي الجزيئي مناطق غنية بالإلكترونات وأخرى فقيرة بها، يُحتمل أن تشارك في التفاعلات بين الجزيئات. أُجريت محاكاة الالتحام الجزيئي باستخدام برنامج MOE 2024 على ثلاثة بروتينات بكتيرية: إنزيم DNA gyrase Bمن الإشريكية القولونية(6KZV) ، وبروتين ربط البنسلين 4 من المكورات العنقودية الذهبية(5TW8) ، وإنزيم لاكاز CotAمن العصوية الرقيقة (1OF0) .أظهر المركب 1 درجات التحام بلغت -6.955، و-5.839، و-5.081 كيلو كالوري/مول على التوالي، مما يشير إلى تفاعلات ربط متوقعة داخل جيوب البروتين المدروسة. كشف تقييم ADMET الحاسوبي عن خصائص فيزيائية وكيميائية مواتية وتوافق مع معايير التشابه الدوائي المعتمدة. ومع ذلك، فقد سلط تثبيط السيتوكروم P450 المتوقع والسمية المحتملة الخاصة بالأعضاء الضوء على مخاوف مهمة تتعلق بالحرائك الدوائية والسلامة. بشكل عام، توفر النتائج توصيفًا أوليًا للمركب المصنّع وتحدد إمكاناته لمزيد من البحث القائم على البنية. يلزم إجراء تقييم بيولوجي تجريبي ودراسات آلية وتقييم للسمية قبل إمكانية إثبات أي أهمية علاجية.

الكلمات المفتاحية: التخليق الكيميائي الانتقائي؛ مشتقات فينيل هيدرازينيل؛ إينامينو إسترات، نظرية الكثافة الوظيفية (DFT)؛ الالتحام الجزيئي.

Introduction:

The continuous emergence and spread of antimicrobial resistance (AMR) represent a major challenge to global healthcare, increasing the difficulty of treating bacterial infections and reducing the effectiveness of existing therapeutic agents. The growing prevalence of multidrug-resistant bacterial pathogens has intensified the demand for the identification and development of structurally diverse chemical entities capable of interacting with biologically relevant molecular targets. Recent global analyses have highlighted the substantial burden associated with bacterial antimicrobial resistance and its projected impact on mortality in the coming decades [1]. Consequently, the exploration of new organic molecular frameworks, supported by modern experimental and computational techniques, remains an important component of early-stage drug discovery.

Nitrogen-containing organic compounds have attracted considerable attention in medicinal and synthetic chemistry because of their structural diversity, chemical reactivity, and ability to establish different types of intermolecular interactions. Among these compounds, enamine-based structures and related β-amino carbonyl derivatives constitute versatile molecular frameworks characterized by conjugated electron-donating and electron-withdrawing functionalities. Such electronic arrangements influence their chemical behavior, molecular stability, and interactions with surrounding environments. Enaminones and related conjugated amino-carbonyl systems have been extensively investigated as synthetic intermediates and molecular scaffolds in the development of compounds with diverse biological properties [2,3]. In particular, the incorporation of nitrogen-containing substituents into conjugated systems provides opportunities for modifying molecular polarity, hydrogen-bonding capacity, and electronic distribution, which are relevant considerations in molecular recognition and structure-based studies.

Phenylhydrazine-derived compounds represent an additional class of nitrogen-containing molecular structures that can be obtained through condensation reactions with suitable carbonyl-containing precursors. These reactions may produce different structural arrangements depending on substrate characteristics, reaction conditions, and the relative reactivity of the available functional groups. In molecules containing more than one carbonyl functionality, chemoselectivity becomes particularly important because preferential reaction at a specific electrophilic center can determine the nature of the

isolated product. Furthermore, the presence of hydrazinyl nitrogen atoms, aromatic rings, and ester functionalities may provide multiple potential sites for hydrogen bonding and other non-covalent interactions. Therefore, the synthesis and detailed characterization of conjugated phenylhydrazinyl derivatives can provide useful information regarding their structural properties and possible interactions with biological macromolecules.

The identification of interactions between small organic molecules and bacterial proteins is an important aspect of structure-based molecular investigation. DNA gyrase B (GyrB), a component of bacterial DNA gyrase, participates in ATP-dependent processes essential for DNA topology regulation and has been investigated as a target for antibacterial drug development [4]. Similarly, penicillin-binding proteins contribute to bacterial cell-wall biosynthesis, and penicillin-binding protein 4 (PBP4) has been associated with mechanisms of β-lactam resistance in Staphylococcus aureus [5]. In contrast, CotA laccase from Bacillus subtilis is a copper-dependent oxidoreductase associated with the bacterial spore coat and oxidative processes [6,7]. Although CotA is not an established antibacterial target comparable to GyrB or PBP4, its structurally characterized binding region provides an additional system for examining the molecular recognition behavior of organic ligands.

Computational chemistry has become increasingly valuable for investigating molecular properties that are not readily accessible through experimental characterization alone. Density functional theory (DFT) provides a theoretical framework for evaluating optimized molecular geometries, electronic energies, charge distributions, and chemical reactivity descriptors. In particular, hybrid exchange–correlation functionals, including the widely employed B3LYP approach, have been extensively applied in quantum chemical investigations of organic systems [8]. Frontier molecular orbital analysis, including the highest occupied molecular orbital (HOMO) and lowest unoccupied molecular orbital (LUMO), can provide insight into the electronic characteristics of a molecule, whereas molecular electrostatic potential maps help identify regions potentially involved in electrophilic, nucleophilic, and hydrogen-bonding interactions.

Complementary to DFT calculations, molecular docking offers a computational approach for exploring possible ligand-binding orientations and identifying non-covalent interactions within protein-binding pockets. Docking simulations can provide preliminary information regarding hydrogen bonding, hydrophobic contacts, and steric compatibility between small molecules and biological targets. However, docking scores represent approximate computational estimates and cannot independently establish experimental binding affinity or biological activity [9]. Accordingly, docking investigations are most informative when integrated with appropriate validation procedures and complementary experimental assessments.

In addition to molecular recognition, physicochemical and pharmacokinetic characteristics are essential considerations during the preliminary evaluation of potential bioactive compounds. Computational prediction platforms such as SwissADME, ADMETlab 3.0, and ProTox 3.0 provide useful tools for estimating molecular drug-likeness, absorption, distribution, metabolism, excretion, and toxicity-related endpoints [10–12]. These approaches allow potentially unfavorable molecular characteristics to be identified at an early stage, although their predictions require experimental validation before conclusions can be drawn regarding pharmacological safety or therapeutic suitability. In this context, the present study investigates the chemoselective synthesis and computational characterization of ethyl 2-(2-phenylhydrazinyl) cyclopent-1-ene-1-carboxylate (1). The synthesized compound was examined using spectroscopic characterization techniques and DFT calculations at the B3LYP/6-31G level to explore its structural and electronic properties. Molecular docking simulations were subsequently performed against three bacterial proteins, namely DNA gyrase B (PDB ID: 6KZV), penicillin-binding protein 4 (PDB ID: 5TW8), and CotA laccase (PDB ID: 1OF0), to investigate possible ligand–protein interactions. Furthermore, in silico ADMET and toxicity analyses were conducted to evaluate the compound's predicted physicochemical, pharmacokinetic, and safety characteristics. By integrating chemical synthesis, quantum chemical calculations, molecular docking, and pharmacokinetic prediction, this investigation aims to establish a preliminary molecular profile of the synthesized phenylhydrazinyl derivative and provide a scientific basis for subsequent experimental investigations.

Experimental and Computational Details:

Materials and Synthetic Procedure:

General Methods and Instrumentation:

All chemicals and solvents were purchased from Sigma-Aldrich (St. Louis, MO, USA) and used as received without further purification. Reaction progress was routinely monitored by thin-layer chromatography (TLC) on silica gel plates using a chloroform/methanol mixture as the eluent. Spectroscopic characterization of the synthesized compound was conducted at the National Research Centre (NRC), Giza, Egypt. $^{1}\mathrm{H\ NMR}$ $(400\ \mathrm{MHz})$ and $^{13}\mathrm{C\ NMR}$ $(100\ \mathrm{MHz})$ spectra were recorded on a

Bruker NMR spectrometer in $CDCl_3$ with tetramethylsilane (TMS) as an internal standard ($\delta = 0$ ppm). Multiplicities are reported as follows: s (singlet), d (doublet), t (triplet), q (quartet), m (multiplet), and br s (broad singlet). Fourier-transform infrared (FT-IR) spectra were recorded on a PerkinElmer 2000 FT-IR system using KBr pellets with wave numbers expressed in cm^{-1}. Melting points (m. p.) were measured in open capillary tubes using a Stuart scientific apparatus and are uncorrected.

Synthesis of Ethyl 2-(2-phenylhydrazinyl) cyclopent-1-ene-1-carboxylate (1):

Equimolar amounts of ethyl 2-oxocyclopentane-1-carboxylate and phenylhydrazine were dissolved in absolute ethanol and refluxed until precipitation was observed. The formed precipitate was isolated by filtration, washed thoroughly with cold ethanol, and recrystallized from ethanol to yield the pure target derivative 1 as an off-white solid (Yield: 19%; m.p. $86 - -87\ ^{\circ}C$).

- **FT-IR** ($KBr, \nu_{max}/cm^{-1}$)**:** $1625.52\ (C = C)$, $1709.42\ (\text{ester } C = O)$, $2974.93\ (\text{aliphatic } C - -H)$, $3029.47\ (= C - -H)$, $3332.64\ (N - -H\ \text{amine})$.
- ^{1}H NMR (400 MHz, $CDCl_3$, δ/ppm)**:** $6.84 - -7.28\ (m,\ 5H,\ Ar - -H)$, $4.23\ (q,\ 2H,\ \underline{CH_2}CH_3)$, $3.77\ (br\ s,\ 2H,\ NH)$, $2.01 - -2.60\ (m,\ 6H,\ CH_2\ \text{of cyclopentene})$, $1.31\ (t,\ 3H,\ CH_2\underline{CH_3})$.
- ^{13}C NMR (100 MHz, $CDCl_3$, δ/ppm)**:** $173.79\ (C = O)$, $153.19\ (C = C - -NH)$, $144.87\ (Ar - -C)$, $129.15, 123.26, 112.98, 80.75, 61.96, 36.85, 25.21, 21.68, 14.18$.
- **APT NMR** ($CDCl_3$, δ/ppm)**:** Up (CH/CH_3): $14.18, 112.98, 120.28, 129.30$; Down ($C_q/CH_2$): $173.13, 154.53, 144.22, 80.78, 61.96, 36.85, 26.31, 21.68$.
- **MS (EI,** m/z**):** M^+ at $246\ (100\%), 200, 172, 95, 92, 77$

Density Functional Theory (DFT) Calculations:

Quantum chemical calculations were performed using Density Functional Theory (DFT) with the B3LYP functional paired with the 6-31G basis set (13) as implemented in the Gaussian 09 software package (14). Full geometry optimization was conducted to obtain the most stable conformation of the synthesized enamine derivative. The convergence criteria for maximum force, root-mean-square (RMS) force, maximum displacement, and RMS displacement met the default thresholds ("YES"). Harmonic vibrational frequency calculations yielded exclusively positive values, confirming that the optimized geometry corresponds to a true local energy minimum and ensuring structural stability (15).

Global reactivity descriptors were derived from conceptual DFT parameters to evaluate the chemical reactivity and kinetic stability of the optimized enamine structure (16). The computed parameters include the highest occupied molecular orbital energy (E_{HOMO}), lowest unoccupied molecular orbital energy (E_{LUMO}), energy gap (ΔE), chemical potential (μ), chemical hardness (η), chemical softness (S), global electrophilicity index (ω), and nucleophilicity index (N). These descriptors were calculated according to Koopmans' theorem using the following equations:

$$\Delta E = E_{LUMO} - E_{HOMO}$$

$$\mu = \frac{E_{LUMO} + E_{HOMO}}{2}$$

$$\eta = \frac{E_{LUMO} - E_{HOMO}}{2}$$

$$S = \frac{1}{2\eta}$$

$$\omega = \frac{\mu^2}{2\eta}$$

$$N = E_{HOMO}(\text{Nucleophile}) - E_{HOMO}(\text{TCE})$$

Additionally, Molecular Electrostatic Potential (MEP/ESP) maps and Mulliken atomic charges were generated over the optimized 3D geometry to determine surface charge distribution, identifying nucleophilic (electron-rich, red regions) and electrophilic (electron-deficient, blue regions) sites responsible for non-covalent binding interactions with biological targets.

Ligand and Receptor Preparation:

The 3D atomic coordinates of the synthesized derivative 1 were built and geometrically optimized in MOE 2024 using the Amber:EHT force field combined with an implicit reaction-field solvation model. Energy minimization was driven until reaching a root-mean-square (RMS) gradient threshold of $0.1\ kcal/mol/A^{\circ}$.

High-resolution X-ray crystal structures of the target bacterial proteins, DNA Gyrase B (*E. coli*, PDB ID: 6KZV), Penicillin-Binding Protein 4 (*S. aureus*, PDB ID: 5TW8), and CotA Laccase (*B. subtilis*, PDB ID: 1OF0), were retrieved from the RCSB Protein Data Bank. Structural preparation was carried out using the QuickPrep module in MOE 2024. Water molecules and non-essential crystallographic additives were removed, while structural copper ions (Cu^{2+}) essential for active-site integrity in 1OF0 were retained. Missing hydrogen atoms were added, 3D protonation states were calculated via Protonate3D at pH 7.0, and tethered energy minimization was applied to relax heavy atoms.

Molecular Docking Simulation and Protocol Validation:

Docking calculations were performed using MOE 2024 to evaluate the binding modes and interaction energies of compound 1 within the active binding sites of 6KZV, 5TW8, and 1OF0. Grid boxes were centered on the binding cavities occupied by the co-crystallized reference ligands. The Triangle Matcher algorithm was selected for conformational placement, and poses were scored using the London dG scoring function, followed by forcefield refinement using the GBVI/WSA dG free-energy model.

To validate the computational protocol, each co-crystallized native ligand was re-docked into its respective binding pocket under identical parameters. The docking methodology was considered reliable as the re-docked poses closely reproduced the experimental crystallographic binding geometries, giving RMSD values well within the acceptable threshold ($\leq 2.0\ \text{A}°$).

In silico ADME and toxicity profiling:

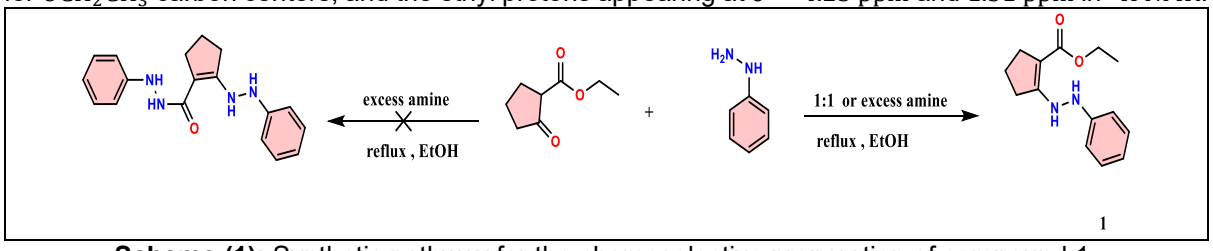
Pharmacokinetic, physicochemical, and toxicity characteristics were assessed to establish drug-likeness. Lipinski's rule compliance and various physicochemical characteristics were estimated using SwissADME. Comprehensive ADME endpoints (absorption, clearance, metabolic stability) were assessed using ADMETLab 3.0, while organ toxicity, cytotoxicity, and LD_{50} values were derived using ProTox 3.0.

Results and Discussion:

Chemical Synthesis and Chemoselectivity:

The target compound, ethyl 2-(2-phenylhydrazinyl) cyclopent-1-ene-1-carboxylate (1), was prepared via a condensation reaction between ethyl 2-oxocyclopentane-1-carboxylate and phenylhydrazine under reflux in ethanol, as depicted in Scheme 1. Notably, the reaction exhibited high chemoselectivity. Conducting the reaction with both an equimolar ratio $(1{:}\,1)$ and an excess of phenylhydrazine consistently yielded the same product (1) without formation of the bis-phenylhydrazide derivative or hydrazide formation at the ester site.

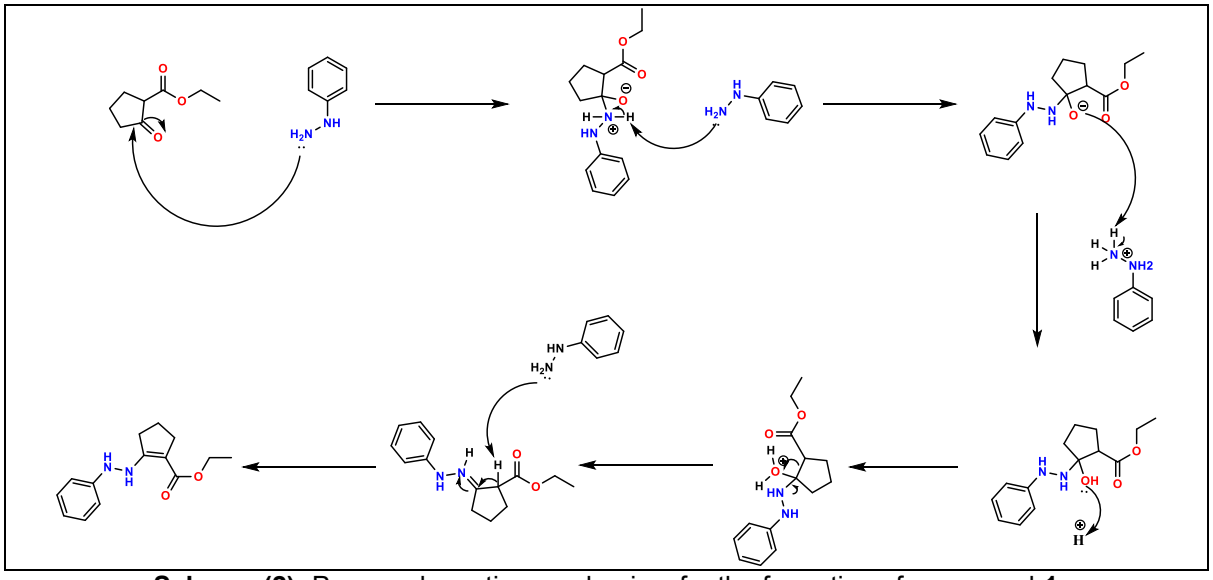
This high chemoselectivity is attributed to the inherently higher electrophilicity of the ketone carbonyl carbon ($C_2 = \text{O}$) compared to the ester carbonyl carbon ($C_1 = \text{O}$), which is resonance-stabilized by the adjacent ethoxy group. Consequently, nucleophilic attack by phenylhydrazine occurs exclusively at the ketone position, leaving the ester functional group completely intact. The preservation of the ester moiety was unequivocally confirmed by spectral data, including the characteristic ester $C = \text{O}$ absorption in FT-IR at $1709.42\ \text{cm}^{-1}$, the ester carbonyl peak in $^{13}\text{C NMR}$ at $\delta = 173.79\ \text{ppm}$, APT peaks for OCH_2CH_3 carbon centers, and the ethyl protons appearing at $\delta = 4.23\ \text{ppm}$ and $1.31\ \text{ppm}$ in $^{1}\text{H NMR}$.



Scheme (1): Synthetic pathway for the chemoselective preparation of compound 1.

Proposed Reaction Mechanism:

As illustrated in **Scheme 2**, the plausible pathway initiates via a selective nucleophilic attack of the primary amino group (NH_2) of phenylhydrazine onto the more reactive ketone carbonyl carbon of ethyl 2-oxocyclopentane-1-carboxylate, forming a tetrahedral intermediate. Subsequent proton transfer and elimination of a water molecule generate the intermediate hydrazone derivative. Tautomerization then yields the highly stable enamine-type derivative 1, stabilized by extended conjugation between the NH lone pair, the $\text{C} = \text{C}$ double bond, and the electron-withdrawing ester group. The unreactive nature of the ester carbonyl toward further nucleophilic substitution, even in the presence of excess phenylhydrazine, confirms that the conjugated enamine-ester framework possesses thermodynamic stability that prevents further addition.



Scheme (2): Proposed reaction mechanism for the formation of compound **1**

Quantum Chemical DFT Analysis:

Thermochemical Analysis and Geometry Optimization:

Geometric optimization and thermochemical analysis of compound 1 executed at the RB3LYP/6-31G level achieved complete convergence with an RMS gradient norm of 0.000005 Hartree/Bohr. Harmonic vibrational frequency calculations yielded zero imaginary frequencies, confirming that the optimized conformation represents a true minimum on the potential energy surface (PES). The total electronic energy (E_{elec}) and thermal free energy (G) were calculated as -804.035392 Hartree and -803.774909 Hartree, respectively. The compound displayed a dipole moment (μ) of 2.8675 Debye and a molecular polarizability (α) of 163.775 a. u.

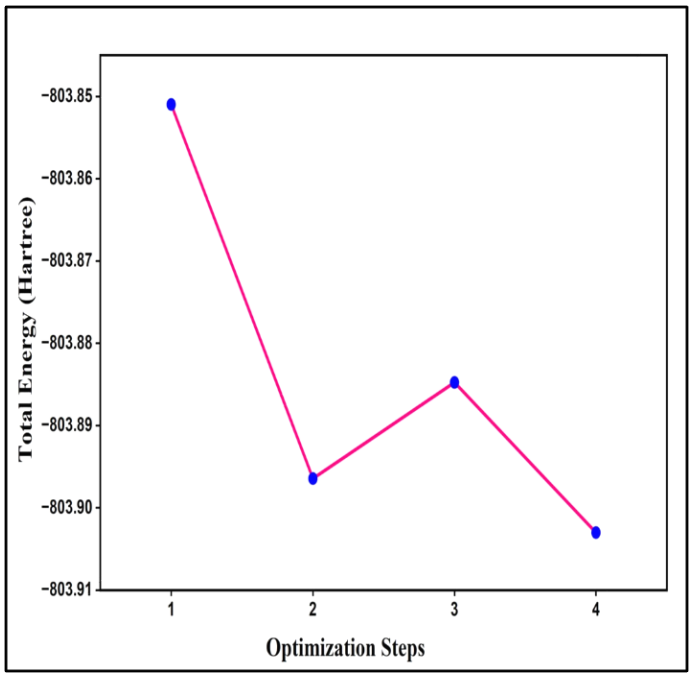


Figure (1): Variation of Total Energy (Hartree) During the Geometry Optimization of Compound 1 at the B3LYP/6-31G Level of Theory.

Frontier Molecular Orbitals (FMOs) and Global Reactivity Descriptors:

The calculated E_{HOMO} and E_{LUMO} for compound **1** were -5.3217 eV $(-0.19557$ Hartree) and -0.8082 eV $(-0.02970$ Hartree), yielding a frontier orbital energy gap (ΔE) of 4.5135 eV. Derived conceptual DFT reactivity descriptors, including chemical hardness ($\eta = 2.2568$ eV), chemical softness

($S = 0.2215\ \mathrm{eV}^{-1}$), chemical potential ($\mu = -3.0650\ \mathrm{eV}$), and global electrophilicity index ($\omega = 2.0818\ \mathrm{eV}$), demonstrate a balanced reactivity profile suitable for active-site binding.

Table (1): Calculated thermochemical, FMO energies, and reactivity descriptors for Compound 1 at the RB3LYP/6-31G level

Parameter	Value (Hartree / a. u.)	Value (eV / Debye)
Total Electronic Energy (E_{elec})	-804.035392	-
Sum of Electronic and Free Energies (G)	-803.774909	-
E_{HOMO}	-0.19557	-5.3217 eV
E_{LUMO}	-0.02970	-0.8082 eV
Energy Gap (ΔE)	0.16587	4.5135 eV
Chemical Hardness (η)	0.082935	2.2568 eV
Chemical Softness (S)	6.0288 a.u	$0.2215\ \mathrm{eV}^{-1}$
Chemical Potential (μ	-0.112635	-3.0650 eV
Global Electrophilicity (ω)	0.07651	2.0818 eV
Dipole Moment (μ_D)	N/A	2.8675 Debye

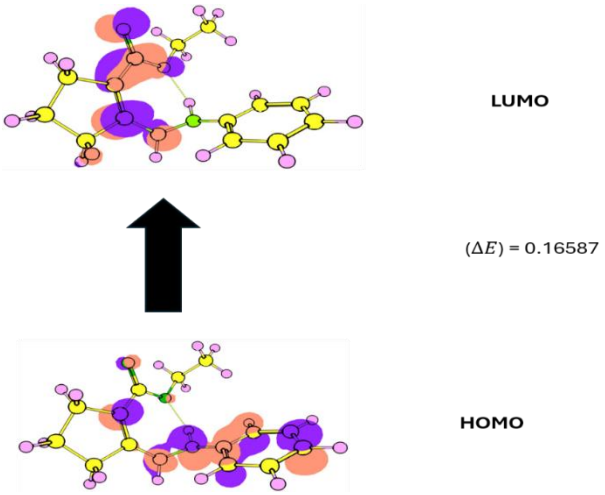


Figure (2): Spatial contour maps of the highest occupied molecular orbital (HOMO) and lowest unoccupied molecular orbital (LUMO) of compound 1 computed at the RB3LYP/6-31G level.

Molecular Electrostatic Potential (MEP) and Mulliken Charge Analysis:

The 3D MEP map reveals electron-rich (red) negative potential localized around the ester carbonyl oxygen atoms, identifying them as hydrogen bond acceptor sites. The electron-deficient (blue) positive regions are concentrated around the amine ($\mathrm{N}--\mathrm{H}$) protons, serving as hydrogen bond donors. Quantitatively, Mulliken atomic charges confirm that the ester oxygen atoms carry substantial negative charges, while the hydrazinyl protons carry significant positive charges, aligning with non-covalent interactions observed in molecular docking

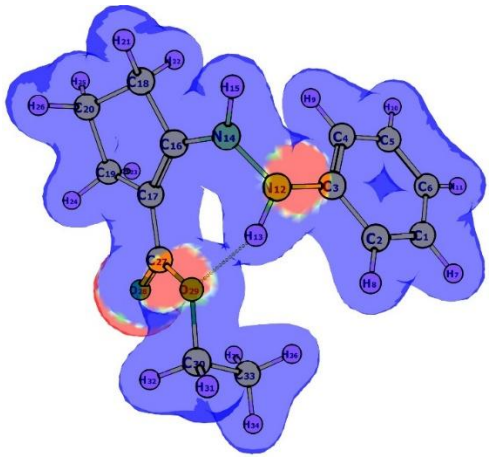


Figure 3. Molecular Electrostatic Potential (MEP) surface topology map of compound 1.

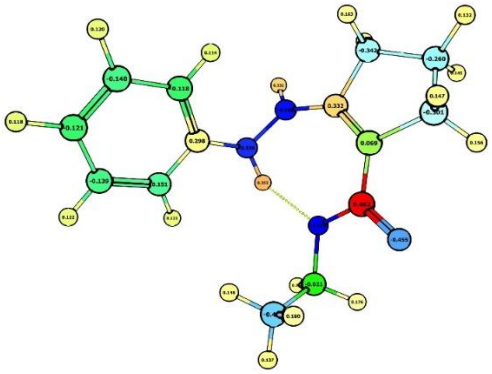


Figure (4): Mulliken atomic charge distribution and dipole moment vector calculated for compound 1 at the RB3LYP/6-31G level

Docking Protocol Validation:

Self-docking of native co-crystallized ligands yielded RMSD values of 1.012 AA for 6KZV, 1.551 AA for 5TW8, and 1.571 AA for 1OF0. All values are below 2.0 AA, validating the docking parameters in MOE 2024.

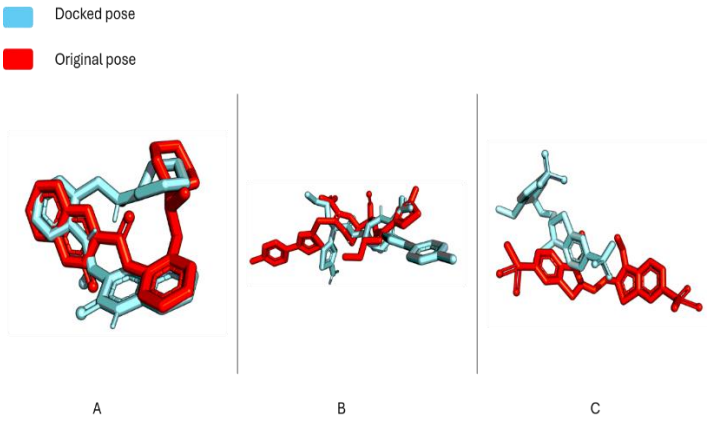


Figure (5): Docking protocol validation showing superimposed docked (cyan) versus native crystal poses (red) for (**A**) 6KZV, (**B**) 5TW8, and (**C**) 1OF0 (RMSD $\leq$ 1.57 AA)

Molecular Docking Analysis of Compound 1:

Table (2): Molecular docking scores, validation RMSD, and detailed binding interactions for Compound 1 and reference ligands within bacterial active sites

PDB	Ligand	S score (kcal/mol)	RMS D (Å)	Atom of compound	Atom of receptor	Involved receptor residues	Type of interaction bond	Distance (Å)	E(kcal/mol)
6KZV	1	-6.955	1.012	N 12 N 24	OD2 O	ASP 73 ASN 46	H-donor H-donor	3.55 3.12	-0.6 -1.9
	Ref Ligand	-7.882	1.257	C24 37 O11 17	O N	ASN 46 GLY 77	H-donor H-acceptor	3.03 2.92	-0.6 -0.5
5TW8	1	-5.839	1.551	O 16 6-ring N8 28 C19 44	OH CA O OE1	TYR 291 ALA 182 ASN 138 GLU 183	H-acceptor pi-H H-donor H-donor	3.03 3.77 3.15 3.55	-1.4 -1.2 -2.3 -0.7
	Ref Ligand	-8.483	1.535	S1 1 O3 7 O3 7 O7 24 O4 12	OH N ND2 OG NH2	TYR 291 SER 116 ASN 141 SER 262 ARG 200	H-acceptor H-acceptor H-acceptor H-acceptor Ionic	3.71 3.01 3.21 3.39 3.91	-1.7 -1.8 -1.1 -0.6 -0.7

				6-ring	NH2	ARG 186	pi-cation	4.19	-2.0
1OFO	1	-5.081	1.571	6-ring	CA	THR 415	pi-H	4.12	-1.1
				6-ring	CG2	THR 415	pi-H	4.44	-0.5
	Ref Ligand	-6.234	1.762	O39 47	NH2	ARG 416	H-acceptor	2.99	-6.1
				O39 47	NE	ARG 416	Ionic	3.87	-0.8
				O39 47	NH2	ARG 416	Ionic	2.99	-4.5

Binding Interaction with DNA Gyrase B (PDB ID: 6KZV):

Compound 1 achieved an S-score of -6.955 kcal/mol against DNA Gyrase B. It establishes a hydrogen bond donor interaction via N12 with Asp73 ($d = 3.55$ A°, $E = -0.6$ kcal/mol), a conserved residue essential for ATP hydrolysis. Hydrophobic interactions by the cyclopentene and phenyl rings further stabilize the binding pose.

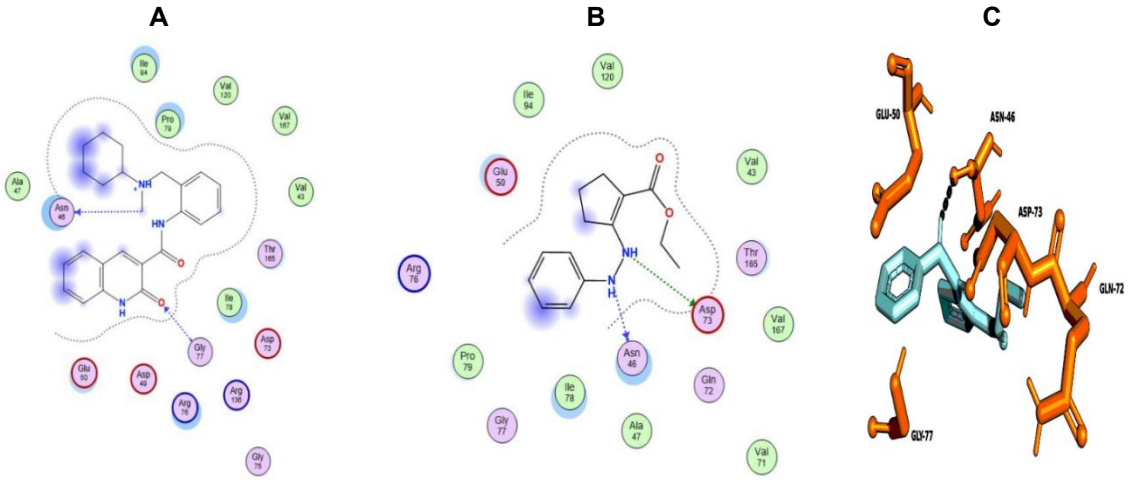


Figure (6): Binding interaction patterns within the active site of DNA Gyrase B (PDB ID: **6KZV**): (**A**) 2D interaction diagram of the co-crystallized reference ligand, (**B**) 2D interaction diagram of **Compound 1**, and (**C**) 3D binding orientation of Compound 1 in the catalytic pocket.

Binding Interaction with Penicillin-Binding Protein 4 (PDB ID: 5TW8):

Compound 1 exhibited a binding score of -5.839 kcal/mol against PBP4. It forms a hydrogen bond acceptor contact via O16 with Tyr291 ($d = 3.03$ A°, $E = -1.4$ kcal/mol), a hydrogen bond donor contact via N8 with Asn138 ($d = 3.15$ A°, $E = -2.3$ kcal/mol), and a π-H contact with Ala182 ($d = 3.77$ A°, $E = -1.2$ kcal/mol).

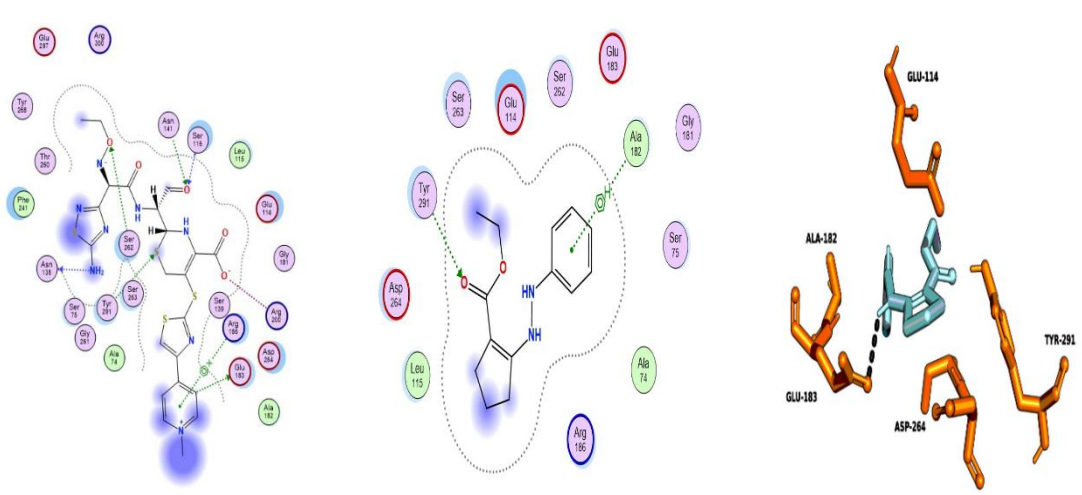


Figure (7): Binding interaction patterns within the active site of Penicillin-Binding Protein 4 (PDB ID: 5TW8): (A) 2D interaction diagram of Ceftaroline (reference ligand), (B) 2D interaction diagram of Compound 1, and (C) 3D binding conformation of Compound 1 inside the binding groove.

Binding Interaction with CotA Laccase (PDB ID: 1OF0):

Compound 1 recorded an S-score of -5.081 kcal/mol against CotA Laccase, anchored primarily through π-H interactions between the phenyl ring and Thr415 ($d = 4.12$ A° and 4.44 A°) near the substrate channel without altering the catalytic copper centers (Cu^{2+}).

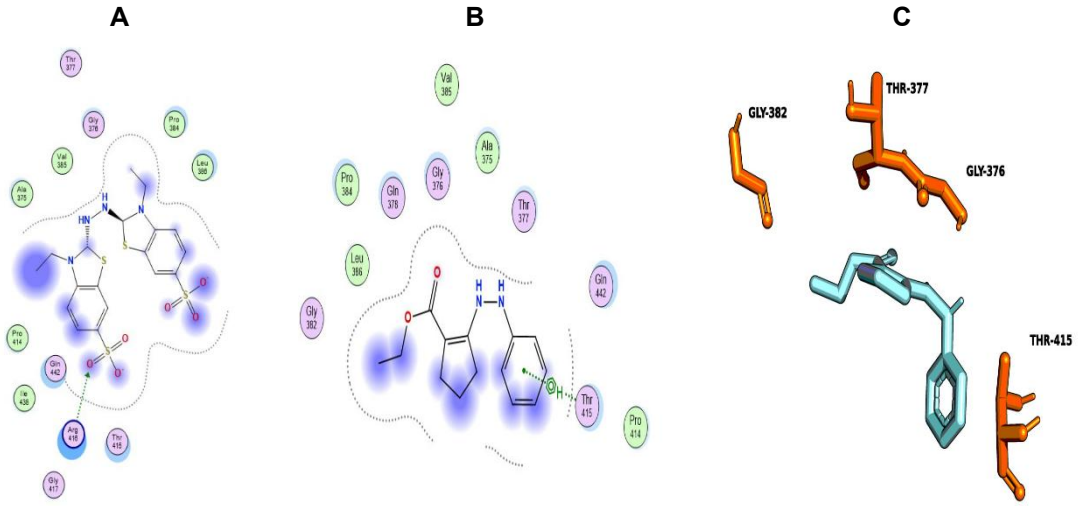


Figure (8). Binding interaction patterns within the active site of CotA Laccase (PDB ID: 1OF0): (A) 2D interaction diagram of ABTS (reference substrate), (B) 2D interaction diagram of Compound 1, and (C) 3D binding representation of Compound 1 near the catalytic copper region

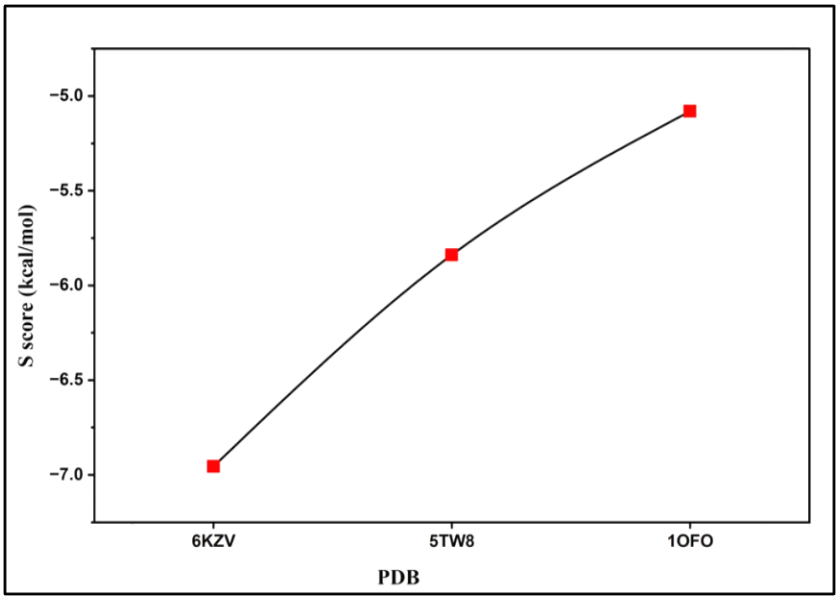


Figure (9): Comparison of Molecular Docking Scores (kcal/mol) of Compound 1 Against Three Target Proteins.

ADME and toxicity profile analysis:

1. **Properties and Drug-Likeness (Table 2):** The compound exhibited favorable physicochemical properties, with a molecular weight of 246.30 g/mol, a topological polar surface area (TPSA) of 50.36 Å², and six rotatable bonds. These characteristics suggest a reasonable balance between molecular flexibility, polarity, and potential membrane permeability. Notably, the compound satisfied all five drug-likeness filters (Lipinski, Ghose, Veber, Egan, and Muegge), with no Lipinski violations. Furthermore, the predicted bioavailability score of 0.55 supports its potential as an orally administered drug candidate. However, experimental validation is required to confirm its actual absorption and bioavailability.
2. **Pharmacokinetic Properties (Table 3):** The ADMET predictions revealed a mixed pharmacokinetic profile. The Caco-2 permeability value (−4.9298) and MDCK permeability (3.08 ×

10^{-5}) provide preliminary indications of membrane transport behavior. The low P-glycoprotein substrate score (0.001338) suggests a limited likelihood of P-gp-mediated efflux. However, high predicted inhibition scores for CYP1A2, CYP2C19, CYP2C9, CYP2D6, and CYP2C8 (0.966–0.999) raise concerns regarding potential drug–drug interactions. The predicted plasma clearance (6.85) and half-life (0.42) also warrant further investigation to clarify the compound's elimination characteristics.

3. **Toxicity Predictions (Table 3):** The predicted LD50 of 1200 mg/kg placed the compound in toxicity class 4, indicating potential acute toxicity. Although hepatotoxicity and cardiotoxicity were classified as inactive, neurotoxicity (0.52), nephrotoxicity (0.63), and respiratory toxicity (0.65) were predicted as active. These findings highlight possible safety concerns that should be considered during further development. Overall, despite its promising drug-likeness properties, the compound requires additional experimental evaluation to establish its pharmacokinetic behavior and safety profile.

Table (3): Physicochemical properties and drug-likeness for Compound.

Physiological properties							Drug likeness properties					
Molecular weight	**Num. heavy atoms**	**Fraction Csp3**	**Num. rotatable bonds**	**Num. H-bond acceptors**	**Num. H-bond donors**	**TPSA**	**Lipinski**	**Ghose**	**Veber**	**Egan**	**Muegge**	**Bio. score**
246.30 g/mol	**18**	**0.36**	**6**	**2**	**2**	**50.36 Å²**	**Yes; 0 violation**	**Yes**	**Yes**	**Yes**	**Yes**	**0.55**

Table (4): In silico ADMET profiling of Compound comprehensive pharmacokinetic and toxicity predictions.

Entry	Compound
Absorption/distribution	
CaCo2	-4.9298
MDCK	3.08E-05
pgb substrate	0.001338
VDss	1.927979
BBB	0.628291
OATP1B1	0.815756
OATP1B3	0.975209
Metabolism	
CYP1A2-inh	0.999816
CYP2C19-inh	0.999018431
CYP2C9-inh	0.999074578
CYP2D6-inh	0.966207862
CYP3A4-sub	0.024728887
CYP2B6-sub	5.02E-05
CYP2C8-inh	0.999643
Excretion	
cl-plasma	6.851133
T1/2	0.422075
Organ toxicity prediction	
Predicted LD50 (mg/kg)	1200
Predicted Toxicity Class	4
Hepatotoxicity	0.57 (Inactive)
Neurotoxicity-	0.52(Active)
Nephrotoxicity-	0.63(Active)
Respiratory toxicity	0.65(Active)
Cardiotoxicity	0.57(Inactive)

Conclusion:

In the present study, ethyl 2-(2-phenylhydrazinyl) cyclopent-1-ene-1-carboxylate (1) was successfully synthesized through a chemoselective condensation reaction between ethyl 2-oxocyclopentane-1-carboxylate and phenylhydrazine. The reaction demonstrated preferential transformation of the ketone functionality while retaining the ester group, providing the targeted conjugated phenylhydrazinyl derivative in 19% isolated yield.

Quantum chemical calculations performed at the B3LYP/6-31G level provided insight into the structural and electronic characteristics of the synthesized compound. Geometry optimization and vibrational frequency analysis supported the stability of the optimized molecular structure, while the calculated HOMO–LUMO energy gap of 4.5135 eV and molecular electrostatic potential distribution provided information regarding electronic properties and potential interaction sites.

Molecular docking investigations revealed predicted interactions between compound 1 and the selected bacterial proteins, with docking scores of −6.955, −5.839, and −5.081 kcal/mol against DNA gyrase B, penicillin-binding protein 4, and CotA laccase, respectively. The observed hydrogen-bonding and hydrophobic interactions suggested molecular compatibility with the investigated binding environments. Nevertheless, the docking scores were less favorable than those of the corresponding reference ligands, and the predicted interactions should not be interpreted as confirmation of biological inhibition.

The in silico ADMET assessment demonstrated favorable physicochemical characteristics and compliance with major drug-likeness criteria. However, the predicted inhibition of several cytochrome P450 enzymes, together with potential neurotoxicity, nephrotoxicity, and respiratory toxicity, indicated important limitations requiring further investigation.

Collectively, these findings establish a preliminary experimental and computational profile of the synthesized phenylhydrazinyl derivative. Future studies should focus on improving the synthetic yield, experimentally investigating antibacterial activity and target inhibition, and evaluating pharmacokinetic and toxicological properties. Such investigations will be essential for determining the biological significance and potential applicability of this molecular framework.

References:

1. GBD 2021 Antimicrobial Resistance Collaborators. (2024). Global burden of bacterial antimicrobial resistance 1990–2021: A systematic analysis with forecasts to 2050. The Lancet, 404(10459), 1199–1226. DOI: 10.1016/S0140-6736(24)01867-1
2. Amaye, I. J., Haywood, R. D., Mandzo, E. M., Wirick, J. J., & Jackson-Ayotunde, P. L. (2021). Enaminones as building blocks in drug development: Recent advances in their chemistry, synthesis, and biological properties. Tetrahedron, 83, 131984. DOI: 10.1016/j.tet.2021.131984
3. Farghaly, T. A., Abo Alnaja, A. M., & Shaaban, M. R. (2021). Recent advances in synthesis and reactions of β-amino-α, β-enones (enaminones). Current Organic Synthesis, 18(7), 639–684. DOI: 10.2174/1570179418666210512015725
4. Ushiyama, F., et al. (2020). Lead identification of 8-(methylamino)-2-oxo-1,2-dihydroquinoline derivatives as DNA gyrase inhibitors: Hit-to-lead generation involving thermodynamic evaluation. ACS Omega, 5(17), 10145–10159. DOI: 10.1021/acsomega.0c00865
5. Alexander, J. A. N., Chatterjee, S. S., Hamilton, S. M., Eltis, L. D., Chambers, H. F., & Strynadka, N. C. J. (2018). Structural and kinetic analyses of penicillin-binding protein 4 (PBP4)-mediated antibiotic resistance in Staphylococcus aureus. Journal of Biological Chemistry, 293(51), 19854–19865. DOI: 10.1074/jbc.RA118.004952
6. Hullo, M. F., Moszer, I., Danchin, A., & Martin-Verstraete, I. (2001). CotA of Bacillus subtilis is a copper-dependent laccase. Journal of Bacteriology, 183(18), 5426–5430. DOI: 10.1128/JB.183.18.5426-5430.2001
7. Enguita, F. J., Marçal, D., Martins, L. O., Grenha, R., Henriques, A. O., Lindley, P. F., & Carrondo, M. A. (2004). Substrate and dioxygen binding to the endospore coat laccase from Bacillus subtilis. Journal of Biological Chemistry, 279(22), 23472–23476. DOI: 10.1074/jbc.M314000200
8. Becke, A. D. (1993). Density-functional thermochemistry. III. The role of exact exchange. The Journal of Chemical Physics, 98(7), 5648–5652. DOI: 10.1063/1.464913
9. Ferreira, L. G., Dos Santos, R. N., Oliva, G., & Andricopulo, A. D. (2015). Molecular docking and structure-based drug design strategies. Molecules, 20(7), 13384–13421. DOI: 10.3390/molecules200713384
10. Daina, A., Michielin, O., & Zoete, V. (2017). SwissADME: A free web tool to evaluate pharmacokinetics, drug-likeness and medicinal chemistry friendliness of small molecules. Scientific Reports, 7, 42717. DOI: 10.1038/srep42717

11. Fu, L., et al. (2024). ADMETlab 3.0: An updated comprehensive online ADMET prediction platform enhanced with broader coverage, improved performance, API functionality and decision support. Nucleic Acids Research, 52(W1), W422–W431. DOI: 10.1093/nar/gkae236
12. Banerjee, P., Kemmler, E., Dunkel, M., & Preissner, R. (2024). ProTox 3.0: A webserver for the prediction of toxicity of chemicals. Nucleic Acids Research, 52(W1), W513–W520. DOI: 10.1093/nar/gkae303
13. Becke, A. D. (1997). Density-functional thermochemistry. V. Systematic optimization of exchange-correlation functionals. The Journal of chemical physics, 107(20), 8554-8560.
14. Frisch, M. J., Trucks, G. W., Schlegel, H. B., Scuseria, G. E., Robb, M. A., Cheeseman, J. R., Scalmani, G., Barone, V., Mennucci, B., Petersson, G. A., Nakatsuji, H., Caricato, M., Li, X., Hratchian, H. P., Izmaylov, A. F., Bloin, O. J., Zheng, G., Sonnenberg, J. L., Hada, M., … Tomasi, J. (2009). Gaussian, Inc., 2009.
15. Cavalli, A., Carloni, P., & Recanatini, M. (2006). Target-related applications of first principles quantum chemical methods in drug design. Chemical reviews, 106(9), 3497-3519.
16. Shahab, S., Hajikolaee, F. H., Filippovich, L., Darroudi, M., Loiko, V. A., Kumar, R., & Borzehandani, M. Y. (2016). Molecular structure and UV–Vis spectral analysis of new synthesized azo dyes for application in polarizing films. Dyes and Pigments, 129, 9-17.